Open-Channel Microfluidic Diodes Based on Two-Tier Junctions

Woo Jin Hyun, Satish Kumar, Lorraine F. Francis, a) and C. Daniel Frisbiea)

Department of Chemical Engineering and Materials Science, University of Minnesota, 421 Washington Ave. SE, Minneapolis, MN 55455, USA

^{a)}Authors to whom correspondence should be addressed: lfrancis@umn.edu and frisbie@umn.edu.

ASTRACT

Precise control of capillary flow is of great importance in open-channel microfluidic technology. We report a compelling strategy to achieve unidirectional liquid flow in open capillary channels. The key flow-rectifying feature is a microfluidic junction between two open channels: a small cross-section, shallower channel and a large cross-section, deeper channel. Liquid flows from the large channel to the small channel, but flow in the opposite direction is blocked at the junction. Experiments and computational analysis show that the rectification follows directly from the Gibbs criterion for flow over step edges. The unidirectional flow behavior is independent of liquid contact angle and surface tension, and also of changes in the channel dimensions, suggesting broad applicability for controlling flow. Specifically, we show that the junction structure can be utilized to facilitate fabrication of electronic devices from functional inks delivered to open capillaries.

MAIN TEXT

Open microfluidics is the science and technology of handling minute amounts of liquids in open microchannels,^{1,2} for applications in chemical analysis,^{3,4} cell and molecular biology,⁵⁻⁷ medical diagnostics,^{8,9} and microelectronics.¹⁰⁻¹⁶ Open channels offer advantages over closed channels for microfluidic systems, including simpler fabrication and more straightforward cleaning and surface modification.¹⁷ In addition, open microfluidic systems typically operate with capillary-driven flow, i.e., without a pump. Such autonomous operation is energy efficient and allows facile miniaturization of microfluidic systems, but the limited degree of liquid flow control necessitates creative strategies to achieve sophisticated function in open channel devices.

An important control element is the microfluidic diode in which fluid flow is unidirectional. Such elements allow simple mixing of fluids without cross contamination of reservoirs, for example.

Microfluidic diodes were initially introduced in closed microfluidic systems with pumps using an elastic valve that deforms and opens in response to liquid pressure. Because of their important function, such diodes have become key building blocks for construction of closed microfluidic systems with high levels of complexity. Previous efforts to rectify capillary flow in open channels have involved engineering the channel sidewalls to reduce capillary pressure. However, the resulting diodes offer rectified flow only for liquids with tight tolerances on liquid contact angle and surface tension. Additionally, the stagnation point in the blocking direction is quite dependent on liquid properties, meaning that sidewall shaping is required over extended distances to achieve complete flow stoppage.

Here we describe compact and robust open capillary microfluidic diodes that employ a two-tier junction. The schematic illustration in Fig. 1(a) depicts the junction structure. Two open channels with different cross-sectional dimensions are joined; a channel (denoted 'S') with a smaller width (w_S) and depth (d_S) is connected to a channel (denoted 'L') with a larger width (w_L) and depth (d_L). This junction halts liquids flowing from S to L [i.e., the 'pinning direction', Fig. 1(b)], but allows liquids to cross from L to S [i.e., the 'free direction', Fig. 1(c)]. The junction structure is created in a silicon wafer by two photolithography cycles (Fig. S1); S is patterned by the first photolithography cycle and L is patterned with a small overlap on S using the second photolithography cycle. The channels are then replicated on other substrates by an imprinting process (Fig. S2). The optical image in Fig. 1(d) shows the diode, associated channels, and liquid reservoirs imprinted in a UV-curable polymer layer on a polyethylene terephthalate (PET) film, which is used for tests in the present study. The reservoirs are large to provide sufficient liquid supply to avoid the influence of the liquid volume on the flow behavior. In addition, the depression at the heart of the junction on the L side [Fig. 1(e)] is generated because this region is etched twice during the silicon master mold fabrication.

The flow rectification properties of the open capillary diode were first tested using a slow moving, viscous liquid (commercial UV-curable resin NOA-73). Videos S1 and S2 show the capillary flow of NOA-73 in the pinning and free directions, respectively, and the liquid front position (x) relative to the reservoir (x = 0) as a function of time (t) is plotted in Figs. 2(a) and 2(b), respectively. As shown in the videos, the liquid does not flow past the S/L junction in the pinning direction (Video S1), but crosses over in the free direction (Video S2). In the pinning direction, the front is stabilized precisely at the junction (Fig. S3).

This unidirectional flow behavior can be explained by considering the junction geometry, the contact angles of the liquid front with the junction walls, and the Gibbs criterion for flow over an edge. Figs. 2(c) and S4(a) illustrate the top and cross-sectional views of the junction and liquid front moving in the pinning direction. The junction possesses three 90° edges (opposing walls and bottom) at the termination of the S channel. According to the Gibbs criterion,²⁴ the liquid front can pass over the sharp edges when its contact angle (θ) exceeds the critical value (θ_{cr}):

$$\theta_{\rm cr} = \theta_{\rm eq} + (180^{\circ} - \alpha) \tag{1}$$

where θ_{eq} and α are the equilibrium contact angle of the liquid on the channel material and the edge angle, respectively, as defined in Fig. S5. For the case of NOA-73, $\theta_{eq} \sim 12^{\circ}$, so $\theta_{cr} \sim 102^{\circ}$. As the leading edges of the liquid front (i.e., the liquid wedges or fingers in the channel corners) reach the S side of the junction [Fig. 2(c)], they become pinned because $\theta \sim \theta_{eq} < \theta_{cr}$. However, liquid flow continues, driven by negative curvature of the front and the corresponding capillary pressure gradient, leading to a buildup of liquid on the S side of the junction and a gradual reduction of curvature of the front. The buildup continues until the curvature of the liquid front is near zero. At this point the capillary pressure gradient disappears, flow ceases, and crucially the contact angle of the liquid at the three edges is still less than θ_{cr} [Figs. 2(c) and S4(a)]. The liquid front becomes firmly pinned. It is important to note that the two-tier structure is essential to the strong pinning effect because the liquid front can advance by wetting in the corners in single depth channels.²³

In the free direction, by contrast, capillary flow never ceases because the capillary pressure gradient does not vanish. Initially, the approaching liquid in the L channel wets the channel surfaces as shown in the first illustration of Fig. 2(d) [Fig. S4(b) for the cross-sectional view]. Due to the front curvature, there is still a significant capillary pressure gradient that continues to drive the flow. Continued liquid filling on the L side of the junction produces the situation shown in the second illustration (see the white arrow) of Fig. 2(d), in which the curvature of the front is still strongly negative, and the increasing liquid volume in the L side of the junction drives a steady increase in θ on the walls and channel bottom. In this situation, where liquid buildup continues, the flow criterion ($\theta > \theta_{cr}$) ultimately occurs and the front is free to cross into the S channel. In short, transport in the free flow direction happens because the geometry of the walls on the L side preserves the capillary-driven flow until $\theta > \theta_{cr}$.

To understand the role of flow dynamics on the junction behavior, we performed additional tests. The different cross-sectional dimensions of S and L result in different flow velocities in the channels because

the capillary flow depends on the channel width and depth. ^{17,25} As shown in Fig. S6, the liquid in L (Video S2) flows faster than the liquid in S (Video S1), implying that the liquid front in the free direction approaches the junction with higher velocity than that in the pinning direction. The faster velocity may help liquid pass over the junction edges due to higher momentum, but we rule out the velocity difference as the reason for the unidirectional flow because of the negligible viscous and inertial forces compared to the surface-tension forces in the system (see the Capillary and Weber numbers in Table S1). This conclusion is confirmed by a test using a 90° junction where S is connected to a sidewall of L to prevent the liquid front from hitting the S entrance directly, as shown in Video S3. Despite losing the momentum due to the indirect route, the liquid crosses from L to S in the 90° junction, similar to the liquid crossing in the straight junction, revealing that the liquid flow in the free direction does not result from the faster velocity.

The mechanism of junction flow can also be probed by examining the influence of the edge angle α on the flow behavior; a test using a 135° junction is shown in Video S4. Unlike the straight [Fig. S7(a)] and 90° [Fig. S7(b)] junctions with sidewall edges having the same α (90°), the 135° junction has sidewall edges with different α values (Fig. S7(c)): 135° for the right sidewall edge ($\theta_{cr} = \theta_{eq} + 45^{\circ}$) and 45° for the left sidewall edge ($\theta_{cr} = \theta_{eq} + 135^{\circ}$). For the free flow direction, the expectation then is that the Gibbs criterion should be met first on the right sidewall with the larger α because it has the lower θ_{cr} . Indeed, while the liquid front in the straight [Fig. S7(d)] and 90° junctions [Fig. S7(e)] crosses over by creating liquid wedges in both corners of the S channel at the same time, the liquid front in the 135° junction [Fig. S7(f)] generates one wedge in the right corner of the S channel first and forms the other wedge in the left corner later when the entire contact line has passed over the bottom edge. Thus, there is a clear dependence of the flow behavior on α that is in accordance with the expectations based on the Gibbs criterion.

Computer simulations based on energy minimization (wetting and surface tension)²⁶ also predict that the junction allows liquid fronts to extend from L into S [Fig. S8(a)], but not from S into L [Fig. S8(b)]. Table S2 summarizes the simulation results using the software Surface Evolver for liquids having different wall contact angles and surface tensions. Surface Evolver predicts direction-dependent liquid behavior regardless of the liquid properties, except for cases exhibiting no capillary action due to poor wetting, i.e., high contact angles.^{1,27} To verify the simulation results, S/L junctions were tested using several inks with different equilibrium contact angles [Fig. 3(a)], surface tensions [Fig. 3(b)], and viscosities [Fig. 3(c)], including aqueous silver ink,²⁸ aqueous poly(3,4-ethylenedioxythiophene):poly(styrene sulfonate) (PEDOT:PSS) ink, and methylene chloride based poly(3-hexylthiophene) (P3HT) ink. These inks leave

behind visible, electrically conductive materials after drying, making it straightforward to assess the spatial extent and continuity of flow. Figs. 3(d)-3(i) and S9 show that for flow in the pinning direction, all inks were stopped precisely at the S/L junction, whereas in the free direction, there was clear crossover in all cases. Furthermore, the microfluidic diodes were not especially sensitive to variations in geometry including width, depth, length, and angle of S and L channels (Figs. S10 and S11). Overall, these results reveal consistent flow behavior in spite of the variation in the liquid properties and channel geometries, demonstrating the broad applicability of the junction for rectifying capillary-driven flow.

Electronics is a significant application field for open microfluidic systems because capillarity-assisted lithography with open channels has facilitated high-resolution and complex patterning of electronic materials. $^{10-16}$ To demonstrate a possible application of the microfluidic diode, electrical resistors were fabricated in channels with S/L junctions. Fig. 4(a) shows a silver conductive line patterned in a simple channel, exhibiting an electrical resistance of $21~\Omega$. By utilizing the junction structure, an electrical resistor was inserted in the conductive line to impart high resistance, as shown in Figs 4(b) and 4(c). When the silver ink was delivered to S [Fig. 4(b)], silver lines were created with a gap equal to the L length because the ink did not flow from L to S. When PEDOT:PSS ink was then delivered to L [Fig. 4(c)], PEDOT:PSS was deposited in L and some part of S because the ink flowed from L to S, making contact with the silver lines. Due to the higher electrical resistivity of the polymer than silver, the PEDOT:PSS pattern in L functions as a resistor, as shown in the inset of Fig. 4(c). As a result, the resistance was significantly increased from $21~\Omega$ [Fig. 4(a)] to $270~k\Omega$ [Fig. 4(b)] by inserting the resistor. Furthermore, Figs. 4(d)-4(f) show that the resistance can be controlled by the L length because the resistance is proportional to L. This suggests a promising strategy to build functional devices in open microfluidic systems for electronic application; this work is ongoing.

Overall, the two-tier capillary diode described here provides highly reproducible and completely rectified liquid flow necessary for many envisioned applications of open microfluidics. Fabrication of the diode structure requires two photolithography steps instead of one used in previous designs, but this extra effort to make the master template is offset by the improved performance and the fact that the master template can be used many times to make molded microfluidic devices by microreplication or imprinting. We anticipate that the diode structure described here can be implemented in many different materials including glass and a variety of plastics, and thus it offers a practical and reliable solution to manipulate capillary flow in a variety of open microfluidic technologies.

SUPPLEMENTARY MATERIAL

See supplementary material for experimental details, Surface Evolver simulation results, dimensionless numbers, more optical/SEM images, and videos for capillary flow in open channels with S/L junctions.

ACKNOWLEDGMENTS

This work was supported by the Multi-University Research Initiative (MURI) program (N00014-11-1-0690) sponsored by the Office of Naval Research. S.K., L.F.F., and C.D.F. also acknowledge financial support through NSF-1634263 and the Xerox Research Centre of Canada. We thank Jennifer A. Lewis and S. Brett Walker for providing silver inks. Parts of this work were performed at the Characterization Facility and the Nano-Fabrication Center of the University of Minnesota. W.J.H. was also supported by the MN Drive program at the University of Minnesota.

REFERENCES

- ¹R. Seemann, M. Brinkmann, E. J. Kramer, F. F. Lange, and R. Lipowsky, Proc. Natl. Acad. Sci. U.S.A. 102, 1848 (2005).
- ²J. Berthier, K. A. Brakke, and E. Berthier, *Open Microfluidics* (Wiley, Hoboken, NJ, USA 2016).
- ³W. H. Ryu, Z. Huang, J. S. Park, J. Moseley, A. R. Grossman, R. J. Fasching, and F. B. Prinz, Lab Chip 8, 1460 (2008).
- ⁴W. Wang, C. Gu, K. B. Lynch, J. J. Lu, Z. Zhang, Q. Pu, and S. Liu, Anal. Chem. 86, 1958 (2014).
- ⁵T. Pfohl, J. H. Kim, M. Yasa, H. P. Miller, G. C. L. Wong, F. Bringezu, Z. Wen, L. Wilson, M. W. Kim, Y. Li, and C. R. Safinya, Langmuir 17, 5343 (2001).
- ⁶F. Piraino, G. Camci-Unal, M. J. Hancock, M. Rasponi, and A. Khademhosseini, Lab Chip 12, 659 (2012).
- ⁷L. J. Barkal, A. B. Theberge, C.-J. Guo, J. Spraker, L. Rappert, J. Berthier, K. A. Brakke, C. C. C. Wang, D. J. Beebe, N. P. Keller, and E. Berthier, Nat. Commun. 7, 10610 (2016).
- ⁸A. W. Martinez, S. T. Phillips, G. M. Whitesides, and E. Carrilho, Anal. Chem. 82, 3 (2010).

- ⁹M. Tani, R. Kawano, Koki Kamiya, and K. Okumura, Sci. Rep. 5, 10263 (2015).
- ¹⁰M. L. Chabinyc, W. S. Wong, K. E. Paul, and R. A. Street, Adv. Mater. 15, 1903 (2003).
- ¹¹C. E. Hendriks, P. J. Smith, J. Perelaer, A. M. J. Van den Berg, and U. S. Schubert, Adv. Funct. Mater. 18, 1031 (2008).
- ¹²H. W. Kim, S. J. Park, B.-K. Lee, and D. S. Kim, Appl. Phys. Lett. 102, 101907 (2013).
- ¹³A. Mahajan, W. J. Hyun, S. B. Walker, G. A. Rojas, J.-H. Choi, J. A. Lewis, L. F. Francis, and C. D. Frisbie, Adv. Electron. Mater. 1, 1500137 (2015).
- ¹⁴W. J. Hyun, F. Zare Bidoky, S. B. Walker, J. A. Lewis, L. F. Francis, and C. D. Frisbie, Adv. Electron. Mater. 2, 1600293 (2016).
- ¹⁵W. J. Hyun, E. B. Secor, C.-H. Kim, M. C. Hersam, L. F. Francis, and C. D. Frisbie, Adv. Energy Mater. 7, 1700285 (2017).
- ¹⁶W. J. Hyun, E. B. Secor, F. Zare Bioky, S. B. Walker, J. A. Lewis, M. C. Hersam, L. F. Francis, and C. D. Frisbie, Flex. Print. Electron. 3, 035004 (2018).
- ¹⁷D. Yang, M. Krasowska, C. Priest, M. N. Popescu, and J. Ralston, J. Phys. Chem. C 115, 18761 (2011).
- ¹⁸Q. Yu, J. M. Bauer, J. S. Moore, and D. J. Beebe, Appl. Phys. Lett. 78, 2589 (2001).
- ¹⁹J. Loverich, I. Kanno, and H. Kotera, Microfluid. Nanofluid. 3, 427 (2007).
- ²⁰D. C. Leslie, C. J. Easley, E. Seker, J. M. Karlinsey, M. Utz, M. R. Begley, and J. P. Landers, Nat. Phys. 5, 231 (2009).
- ²¹H. A. Stone, Nat. Phys. 5, 178 (2009).
- ²²M. L. Blow, H. Kusumaatmaja, and J. M. Yeomans, J. Phys. Condens. Matter 21, 464125 (2009).
- ²³J. Feng and J. P. Rothstein, J. Colloid Interface Sci. 404, 169 (2013).
- ²⁴J. W. Gibbs, *The Scientific Papers of J. Willard Gibbs* (Dover, New York 1961).
- ²⁵F. F. Ouali, G. McHale, H. Javed, C. Trabi, N. J. Shirtcliffe, and M. I. Newton, Microfluid. Nanofluid. 15, 309 (2013).
- ²⁶K. A. Brakke, Exp. Math. 1, 141 (1992).
- ²⁷P. Concus and R. Finn, Proc. Natl. Acad. Sci. U.S.A. 63, 292 (1969).
- ²⁸S. B. Walker and J. A. Lewis, J. Am. Chem. Soc. 134, 1419 (2012).

FIGURES

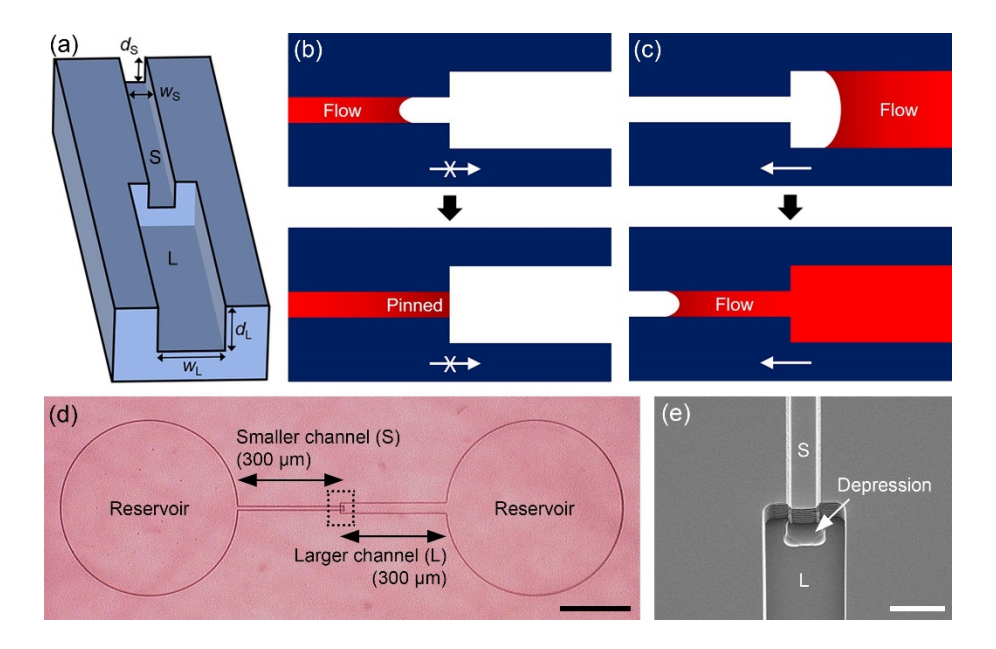


FIG. 1. (a) Three-dimensional illustration for an open capillary microfluidic diode. A channel (S) with a smaller width (w_S) and depth (d_S) is connected to a channel (L) with a larger width (w_L) and depth (d_L) . (b) Schematic diagram for liquid flow from S to L (pinning direction). (c) Schematic diagram for liquid flow from L to S (free direction). (d) Optical image of an open channel with the S/L junction imprinted on a plastic substrate. (e) Tilted SEM image for the junction in the dotted box in (d). Scale bars are 200 μm in (d) and 20 μm in (e).

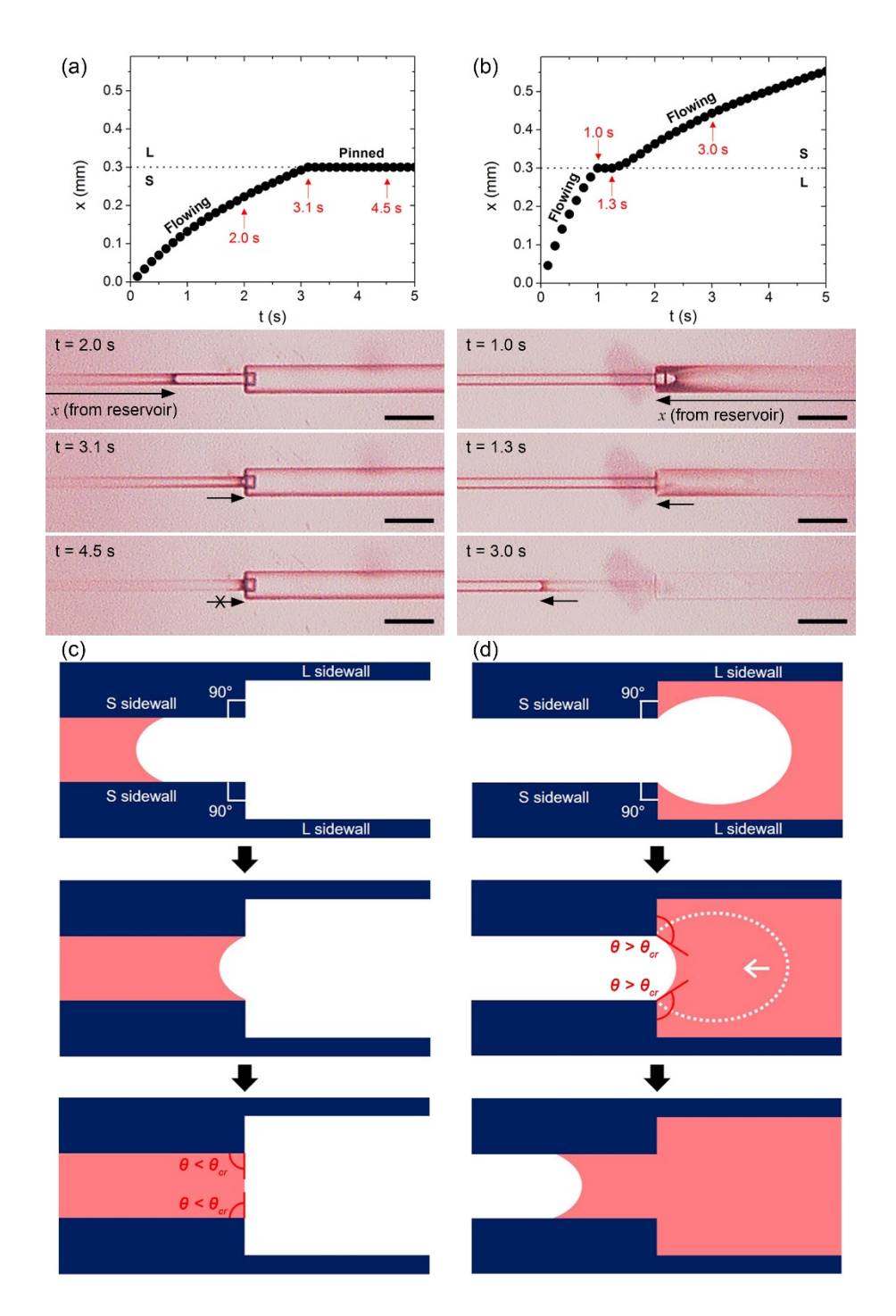


FIG. 2. (a) Liquid front position (x) from the reservoir (x = 0) as a function of time (t) for the NOA-73 flow in the pinning direction, and frames (Video S1) at $t = 0.5 \times 0.5$

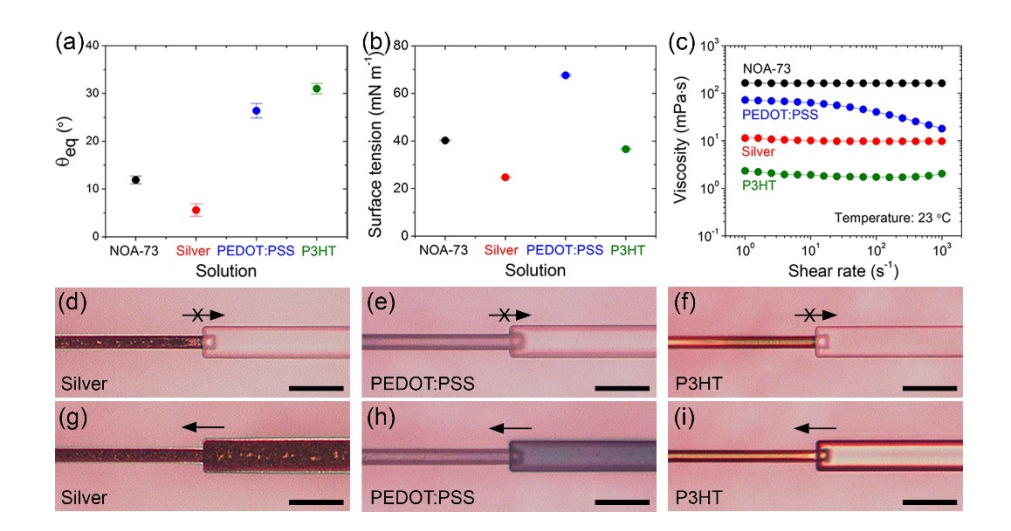


FIG. 3. (a) Equilibrium contact angle (θ_{eq}) on the plastic substrate, (b) surface tension, and (c) shear viscosity for electronic inks (silver, PEDOT:PSS, and P3HT) and NOA-73. (d-f) Optical images of the channels with electronic materials deposited by the ink flow in the pinning direction. (g-i) Optical images of the channels with electronic materials deposited by the ink flow in the free direction. w_S , d_S , w_L , and d_L for the channels in (d-i) are 10, 3.4, 30, and 9.4 µm, respectively. All scale bars are 50 µm.

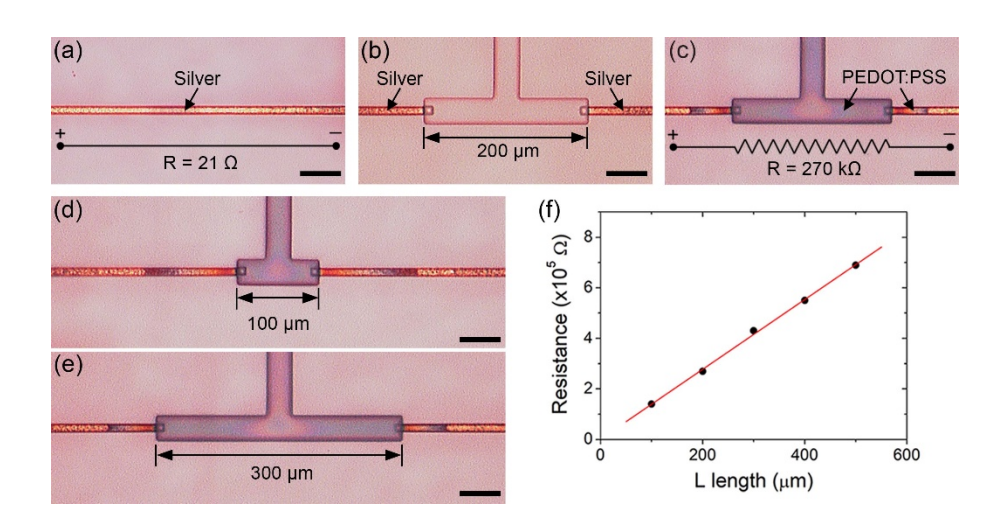


FIG. 4. (a) Optical image of a silver conductive line patterned in a channel. (b,c) Optical images of a channel with two junctions after pattering silver and PEDOT:PSS, respectively. (d,e) Optical images of electrical resistors with different L lengths. (f) Resistance of the fabricated electrical resistors as a function of the L length. All scale bars are 50 μm.

Supplementary Material

Open-Channel Microfluidic Diodes Based on Two-Tier Junctions

Woo Jin Hyun, Satish Kumar, Lorraine F. Francis, and C. Daniel Frisbiea)

Department of Chemical Engineering and Materials Science, University of Minnesota, 421 Washington Ave. SE, Minneapolis, MN 55455, USA

^{a)}Authors to whom correspondence should be addressed: lfrancis@umn.edu and frisbie@umn.edu.

EXPERIMENTAL DETAILS

Preparation of two-tier junctions in a silicon wafer.

A silicon master mold was prepared by two photolithography cycles (Fig. S1). For the first photolithography cycle, a 4-in silicon wafer was pre-baked at 115 °C for 1 min, vapor-coated with hexamethyldisilazane (KMG Electronic Chemicals) for 3 min, and spin-coated with photoresist (Microposit S1813, Dow) at 2000 rpm for 30 s. After soft-baking at 115 °C for 1 min and UV exposure with a photomask using a mask aligner (MA6, Karl Suss), the wafer was immersed in a developer (Microposit 351, Dow) diluted with deionized water (1:5 v/v) for 40 s, and rinsed with deionized water. The features were then etched by reactive ion etching (320, Surface Technology Systems), followed by rinsing the photoresist with acetone, ethanol, isopropanol, and deionized water, sequentially. For the second photolithography cycle, the silicon wafer was prebaked at 200 °C for 5 min, vapor-coated with hexamethyldisilanzane for 3 min, and spin-coated with photoresist (AZ 9260, MicroChemicals) at 300 rpm for 10 s and at 3000 rpm for 60 s, sequentially. After soft-baking at 110 °C for 165 s, the photoresist was exposed to UV light through a photomask using the mask aligner. The wafer was immersed in a developer solution (AZ 400K, Merck Performance Materials) diluted with deionized water (1:4 v/v) for 4 min, and rinsed with deionized water. The features were then etched by reactive ion etching (SLR-770, Plasma-Therm), and the photoresist was rinsed with acetone, ethanol, isopropanol, and deionized water, sequentially. Finally, the silicon wafer was submerged in piranha solution of hydrogen peroxide and sulfuric acid (1:1 v/v) on a 120 °C hotplate for 30 min to clean residual photoresist.

Imprinting process (Fig. S2).

For fabrication of polydimethylsiloxane (PDMS) stamps, the silicon master mold was silane-treated in a vacuum chamber with 0.2 mL of trichloro(1H,1H, 2H,2H-perfluorooctyl)silane (Sigma-Aldrich) for 4 h. A PDMS monomer and its curing agent (10:1 w/w, Sylgard 184, Dow Corning) was poured onto the master mold. After curing in an oven at 70 °C for 3 h, the PDMS stamp was peeled off from the master mold and post-cured in an oven at 120 °C for 2 h. Following the preparation of the stamp, a UV-curable polymer (NOA-73, Norland Products) was poured on a PET film that was plasma-treated (PDC-32G, Harrick Plasma) for 3 min, and pressed by the PDMS stamp. After the photopolymer was exposed to UV light (wavelength: 365 nm, LED SPOT 100, Dr. Hönle AG) for 90 s, the stamp was delaminated from the cured photopolymer.

Electronic inks and deposition.

Silver and PEDOT:PSS (PH1000) inks were obtained from Electroninks and Heraeus, respectively. P3HT was purchased from Rieke Metals, and a P3HT ink was prepared by dissolving the polymer in

1,2-dichlorobenzene (Sigma-Aldrich) with a concentration of 6 mg mL⁻¹. After plasma treatment of the substrates for 60 s, the inks were delivered to reservoirs employing a custom-built drop-on-demand inkjet printer with an 80 μ m diameter nozzle (MJ-AT-01, MicroFab) at room temperature. For the inkjet printing, a unipolar waveform (rise/dwell/fall time: 5/30/5 μ s) was used at a drive voltage and frequency of 120 V and 1 kHz, respectively.

Characterization.

Depth of the channels was measured using a surface profiler (P-16, KLA-Tencor). The prepared channels and electronic materials (silver, PEDOT:PSS, and P3HT) deposited in the channels were observed using a digital microscope (KH-7700 with a OL-140 II lens, Hirox) and a scanning electron microscope (JSL-6500, JEOL). Videos for the liquid flows in the channels were recorded employing the digital microscope at 15 frames per second. Shear viscosity of the test liquids was measured using a rheometer (AR-G2, TA instrument) with a 40 mm, 2° steel cone and plate geometry at a temperature of 23°C. Current-voltage curves of silver conductive lines patterned in the channels were obtained using source meters (236 and 237, Keithley). Equilibrium contact angle and surface tension of the liquids were measured employing a drop shape analyzer (DSA-30, KRÜSS).

SUPPLEMENTAL FIGURES AND TABLES

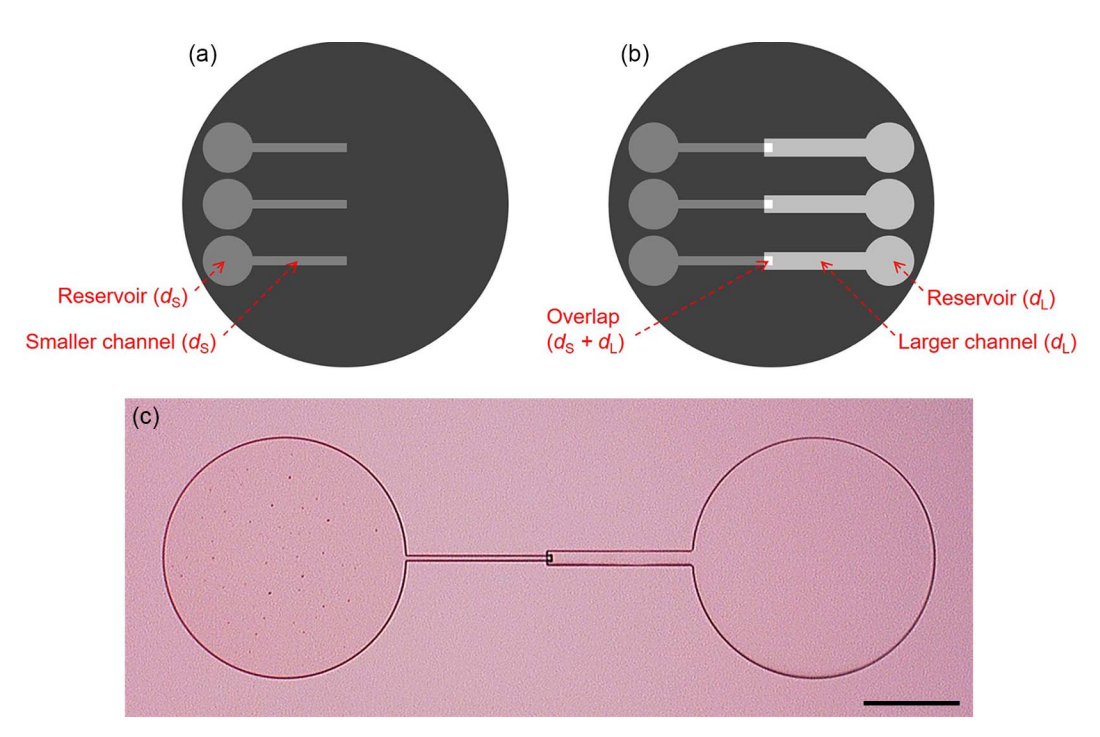


Fig. S1. Preparation of open channels with the S/L junction structure on a silicon wafer. (a) Smaller channels and reservoirs are etched to a depth of d_S by first photolithography step. (b) Larger channels and reservoirs are etched to a depth of d_L by second photolithography step, with a small overlap on the smaller channels. The overlap region is etched twice, generating a depression (depth from the silicon wafer top surface: $d_S + d_L$) in the larger channel. (c) Optical image of the open channel with the junction structure on a silicon wafer. w_S , d_S , w_L , and d_L of the channel are 10, 3.4, 30, and 9.4 μm, respectively. The scale bar is 200 μm.

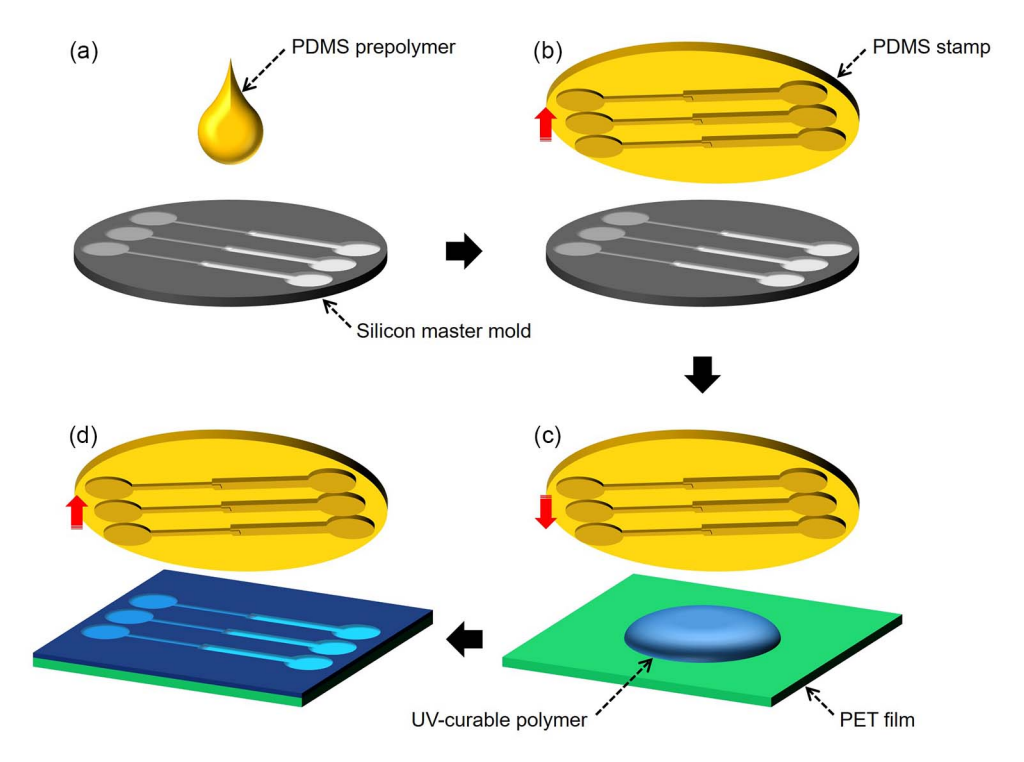


Fig. S2. Imprinting process for plastic substrates. (a) A mixture of PDMS prepolymer and its curing agent is poured onto a silicon master mold. (b) After curing, the PDMS stamp is peeled off from the mater mold. (c) UV-curable polymer is coated on a PET film and pressed by the PDMS stamp. (b) The stamp is delaminated from the polymer coating after UV curing of the photopolymer.

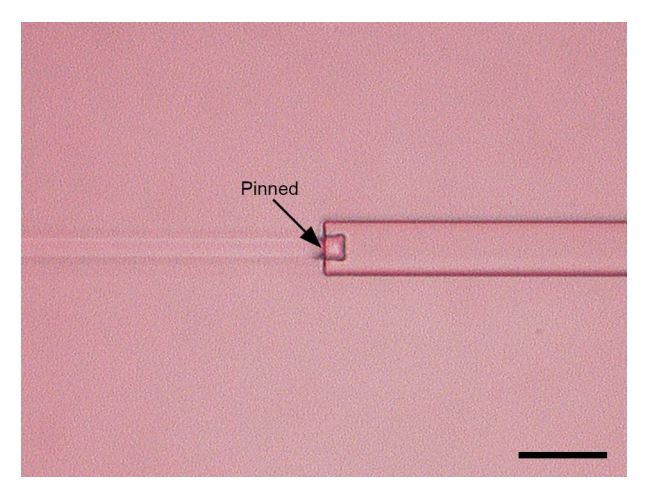


Fig. S3. Optical image of NOA-73 pinned by the junction diode for 2 h. The sample was stored for 2 h in the dark to avoid curing of NOA-73 (UV-curable resin). The scale bar is 50 μ m.

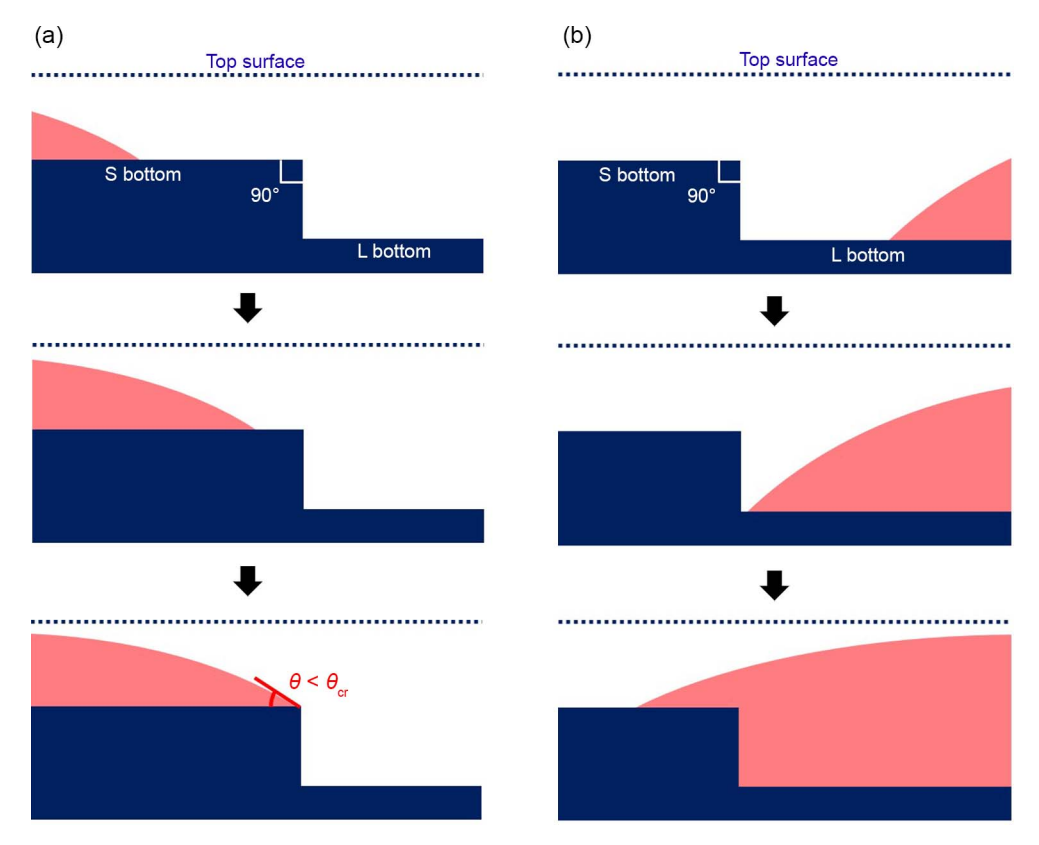


Fig. S4. Cross-sectional illustrations for the channel and liquid front flowing in (a) pinning and (b) free directions. Cut is taken down the center of the channel.

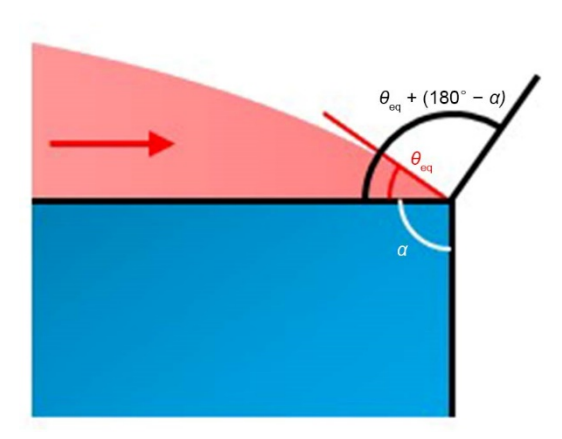


Fig. S5. Illustration for a liquid front (red) at a sharp edge (blue) with an angle of α . θ_{eq} indicates the equilibrium contact angle of the liquid.

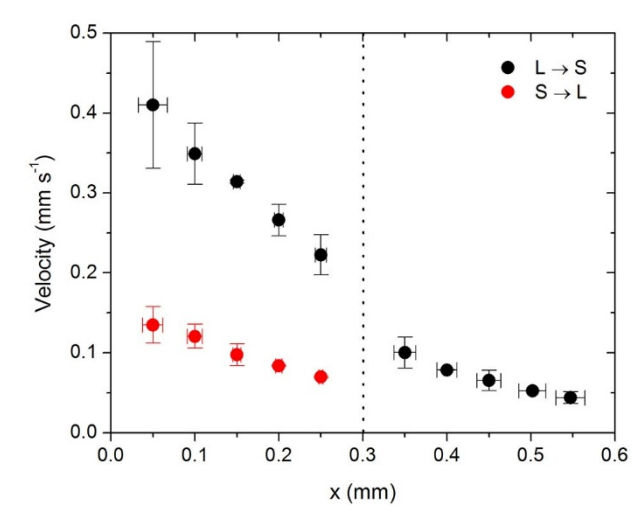


Fig. S6. Velocity of the liquid front as a function of x for the NOA-73 flow in the pinning (red, Video S1) and free (black, Video S2) directions. The dotted line indicates the position of the S/L junction.

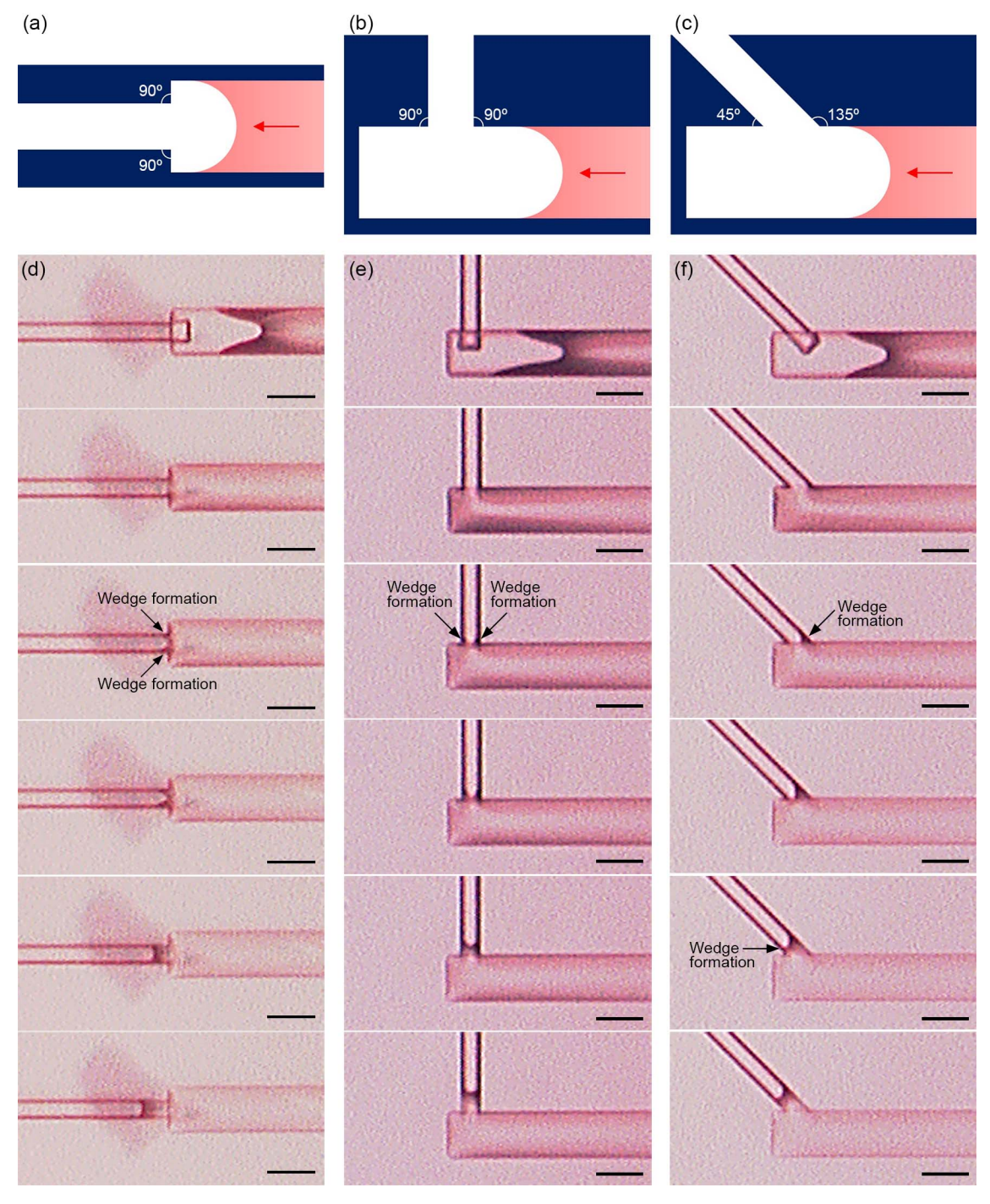


Fig. S7. Illustrations for (a) straight, (b) 90°, and (c) 135° junctions. Sequential frames of Videos (d) S2, (e) S3, and (f) S4. All scale bars are 30 μ m.

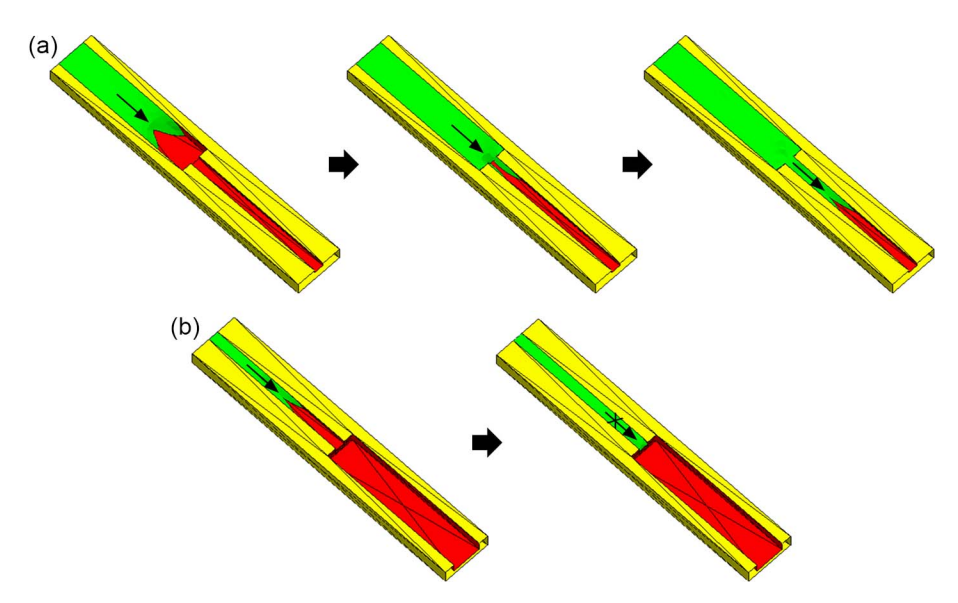


Fig. S8. (a) The liquid in L extends its front into S. (b) The liquid in S does not extend its front into L. The liquid, channel top surface, and bottom and sidewalls are in green, yellow, and red, respectively.

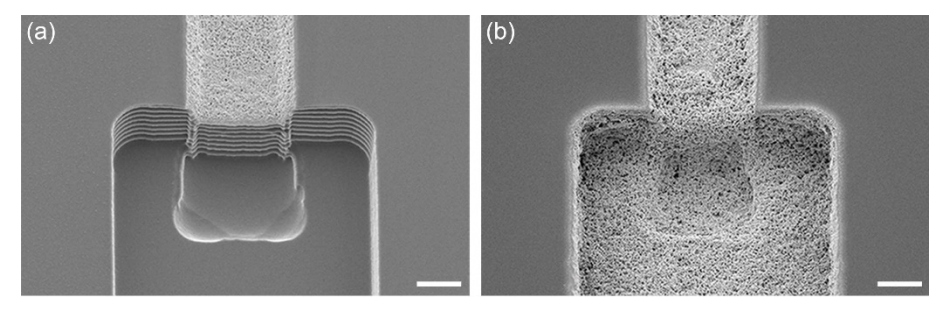


Fig. S9. (a) SEM image of the channels with silver deposited by the ink flow in the pinning direction. (b) SEM image of the channels with silver deposited by the ink flow in the free direction. w_S , d_S , w_L , and d_L for the channels are 10, 3.4, 30, and 9.4 μ m, respectively. All scale bars are 5 μ m.

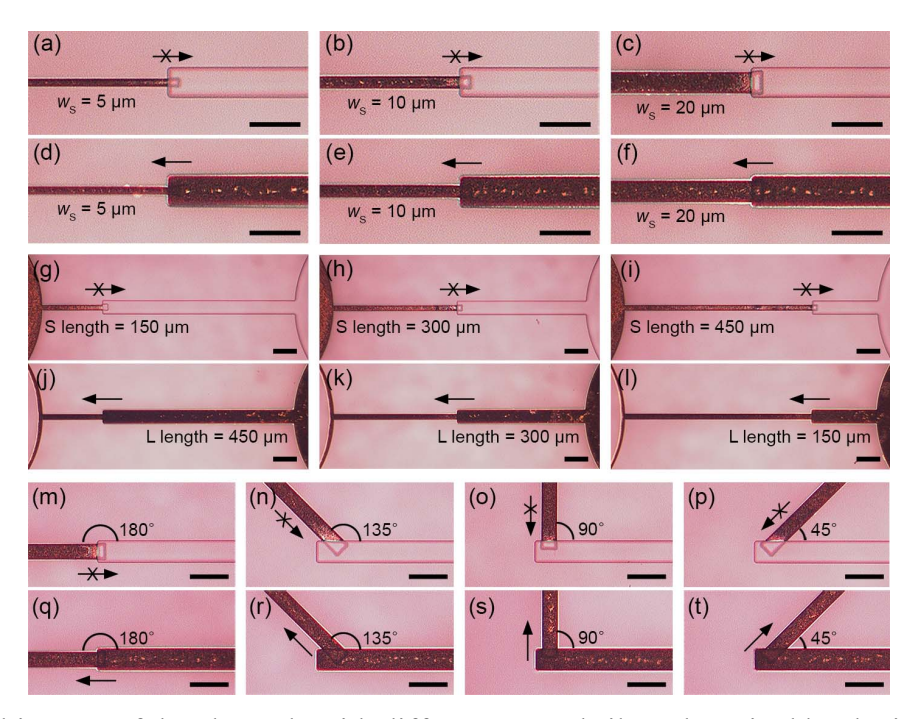


Fig. S10. Optical images of the channels with different w_S and silver deposited by the ink flow in the (a-c) pinning and (d-f) free directions. Optical images of the channels with different lengths of S and L and silver deposited by the ink flow in the (g-i) pinning and (j-l) free directions. Optical images of the channels with different angles between S and L and silver deposited by the ink flow in the (m-p) pinning and (q-t) free directions. w_S , d_S , w_L , and d_L are w_S (as noted), 3.4, 30, and 9.4 μm, respectively, in (a-f), 10, 3.4, 30, and 9.4 μm, respectively, in (g-l), and 20, 3.4, 30, and 9.4 μm, respectively, in (m-t). All scale bars are 50 μm.

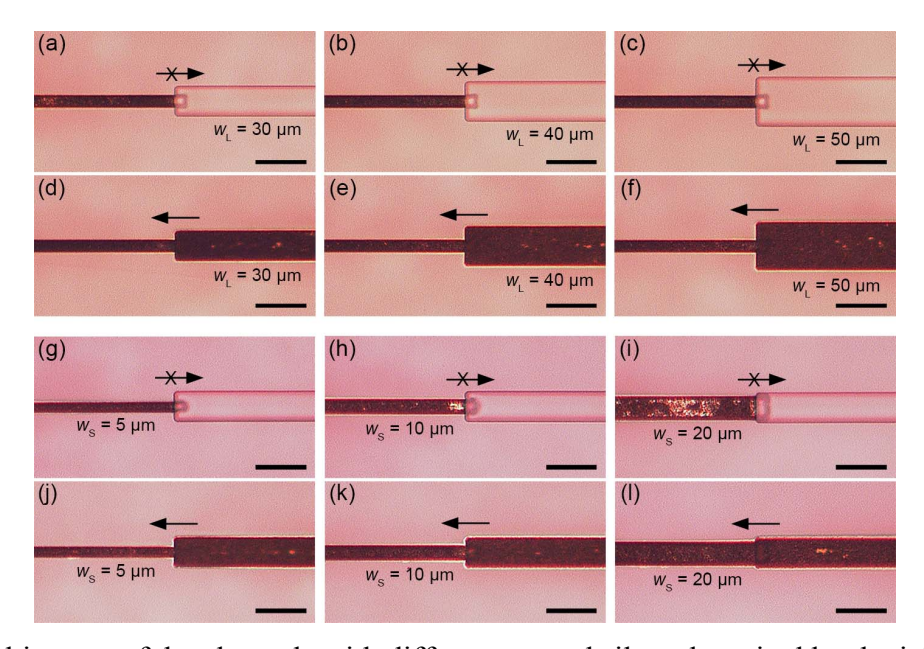


Fig. S11. Optical images of the channels with different w_L and silver deposited by the ink flow in the (a-c) pinning and (d-f) free directions. Optical images for the channels with larger d_S and d_L [compared to those in Figs. S10(a)-S10(f)] and silver deposited by the ink flow in the (g-i) pinning and (j-l) free directions. w_S , d_S , w_L , and d_L are 10, 3.4, w_L (as noted), and 9.4 μm, respectively, in (a-f), and w_S (as noted), 5.9, 30, and 14.3 μm, respectively, in (g-l). All scale bars are 50 μm.

Table S1. Dimensionless numbers for capillary flow of the test liquids in the channel.

Dimensionless number	NOA-73	Silver	PEDOT:PSS	Р3НТ	
(Capillary number) $Ca = \frac{\mu V}{\gamma} = \frac{\text{Viscous force}}{\text{Surface tension force}}$	< 2.0 × 10 ⁻³	< 4.0 × 10 ⁻³	< 1.0 × 10 ⁻²	< 5.4 × 10 ⁻⁴	
(Weber number) $We = \frac{\rho V^2 D_{\text{H}}}{\gamma} = \frac{\text{Inertial force}}{\text{Surface tension force}}$	< 1.7 × 10 ⁻⁷	< 1.0 × 10 ⁻⁴	< 3.3 × 10 ⁻⁵	< 8.1 × 10 ⁻⁵	
(Reynolds number) $Re = \frac{\rho V D_{\text{H}}}{\mu} = \frac{\text{Inertial force}}{\text{Viscous force}}$		< 2.5 × 10 ⁻²	< 3.3 × 10 ⁻³	< 1.5 × 10 ⁻¹	
Values for calculation					
μ: viscosity (mPa·s)	160	10	< 70	2	
ρ: density (kg m ⁻³)	1.2×10^{3}	1.1×10^{3}	1.0×10^{3}	1.3×10^{3}	
γ: surface tension (mN m ⁻¹)	40	25	68	37	
V: velocity (mm s ⁻¹)	< 0.5 < 10				
$D_{\rm H}$: hydraulic diameter	4wd/(2d+w)				

Table S2. Surface Evolver simulation results with varying the liquid contact angle and surface tension.

Contact angle (°)	Surface tension (mN m ⁻¹)	Flow from S to L (pinning direction)	Flow from L to S (free direction)	
1 10 20	40	Pinning	Spreading	
40 50		No capillarity	No capillarity	
1	10 20 80		Spreading	
10	10 20 80	Pinning		
40	10 20 80			

Video S1. Flow (× 0.5 speed) of NOA-73 from S to L in the channel. w_S , d_S , w_L , and d_L are 10, 3.4, 30, and 9.4 μ m, respectively.

Video S2. Flow (× 0.5 speed) of NOA-73 from L to S in the channel. w_S , d_S , w_L , and d_L are 10, 3.4, 30, and 9.4 μ m, respectively.

Video S3. Flow (× 0.5 speed) of NOA-73 from L to S in the channel where S is connected to a sidewall of L with an angle of 90°. w_S , d_S , w_L , and d_L are 10, 3.4, 30, and 9.4 μ m, respectively.

Video S4. Flow (× 0.5 speed) of NOA-73 from L to S in the channel where S is connected to a sidewall of L with an angle of 135°. w_S , d_S , w_L , and d_L are 10, 3.4, 30, and 9.4 μ m, respectively.